AIAA JOURNAL
Vol. 41, No. 8, August 2003

Inflow Boundary Conditions for Hybrid Large Eddy/Reynolds Averaged Navier–Stokes Simulations

Xudong Xiao,* J. R. Edwards,† and H. A. Hassan‡
North Carolina State University, Raleigh, North Carolina 27695-7910
and
R. A. Baurle§
Taitech, Inc., Beavercreek, Ohio 45430-1065

Inflow boundary conditions are developed for hybrid large-eddy simulation (LES)/Reynolds-averaged Navier–Stokes approaches. They are based on an extension of the rescaling-reintroducing method developed for LES to a hybrid scheme. A blending function is used to shift the turbulence closure from a k–ζ model near the wall to a k–Δ subgrid-scale model away from the wall. The approach was tested for a flat plate and then applied to the study of a 25-deg compression–expansion ramp for a Mach number of 2.88 and a Reynolds number of 3.24×10^7/m. In general, improvements over the k–ζ model were noted in the recovery region. The significance of this work is that it provides a way for LES methods to address flows at a high Reynolds number.

Nomenclature

k	=	turbulent kinetic energy, m^2/s^2
p	=	pressure, N/m^2
T	=	temperature, K
U	=	mean velocity in x direction, m/s
u	=	instantaneous velocity in x direction, m/s
u_τ	=	friction velocity, m/s
x, y, z	=	coordinate directions in physical space, m
α_1	=	model constant
$\Gamma, \Gamma_1, \Gamma_2$	=	blending functions
$\Delta, \Delta_m, \Delta_v$	=	grid cell size, m
δ	=	boundary-layer thickness, m
ζ	=	enstrophy, $1/s^2$
ν	=	laminar kinematic viscosity, m^2/s
ν_t	=	turbulent kinematic viscosity, m^2/s
ρ	=	density, kg/m^3
τ_w	=	wall stress, N/m^2

Subscripts

inf	=	inflow station
rec	=	recycle station
t	=	turbulence
w	=	wall
∞	=	freestream

Superscripts

inn	=	inner region
out	=	outer region
$''$	=	fluctuations

Received 2 November 2002; presented as Paper 2003-0079 at the AIAA 41st Aerospace Sciences Meeting, Reno, NV, 6–9 January 2003; revision received 17 March 2003; accepted for publication 21 March 2003.

*Research Assistant, Department of Mechanical and Aerospace Engineering. Student Member AIAA.

†Associate Professor, Department of Mechanical and Aerospace Engineering. Senior Member AIAA.

‡Professor, Department of Mechanical and Aerospace Engineering. Associate Fellow AIAA.

§Senior Research Scientist, Computational Fluid Dynamics Group; currently Aerospace Engineer, Hypersonic Airbreathing Propulsion Branch, NASA Langley Research Center, Hampton, VA 23681-2199. Senior Member AIAA.

Introduction

RECENT attempts at coupling large-eddy simulation (LES) approaches with Reynolds-averaged Navier–Stokes (RANS) solvers to overcome resolution issues in the near-wall regions at high Reynolds numbers have focused on blending of the two schemes, for example, Refs. 1–7. In most cases the boundary conditions employed consisted of traditional RANS boundary conditions with imposed random fluctuations that can recover the turbulent stresses. It became clear later[8–10] that such boundary conditions only work well in situations where there is a clear demarcation between regions treated as LES (such as free-shear layers and massive separation zones) and those treated as RANS (such as near-wall flows). When a clear geometric demarcation does not exist between the two regions, which is the case in shock-wave/boundary-layer interactions, a different approach is needed. To avoid discarding the resolvable component of turbulent kinetic energy in fine grid regions, Batten et al.[9] proposed the use of three additional stochastic partial differential equations for the velocity fluctuations. Arunajatesan et al.[10] used an interface region in which the RANS boundary layer was transformed into an LES boundary layer using the recycling method of Urbin and Knight.[11]

It appears that in order for hybrid LES/RANS approaches to perform for general flows of interest appropriate boundary conditions for hybrid schemes must be compatible with both LES and RANS approaches. Imposing random fluctuations that reproduce turbulent stresses on RANS boundary conditions is not a viable approach because the resulting fluctuations are not consistent with the Navier–Stokes equations. Moreover, the procedure requires a long transition region to develop large-scale fluctuations. Because of this, attention is focused here on extending the rescaling-reintroducing procedures developed for LES and DNS applications in Refs. 11–13 to hybrid LES/RANS schemes. The extension is carried out in such a way so as to be used with any RANS model. It is illustrated here using the k–ζ model[14] and in Ref. 15 using Menter's supersonic transport model.[16]

Rather than use a variation of approaches suggested in Refs. 1 and 2, the zonal approach developed by Fan et al.[6,8] is employed. This approach utilizes a blending function that, depending on the flow properties, shifts the model from RANS behavior near the wall to LES behavior away from the wall. The use of the k–ζ RANS model was motivated by the desire to use a blending function that has no explicit dependence on the wall distance. As can be noted in Ref. 14, the k–ζ model does not employ wall or damping functions and is coordinate-system invariant.

The inflow boundary conditions are developed first for a LES/RANS hybrid scheme using supersonic flow over a flat plate

and then applied to the 25-deg compression–expansion ramp of Zheltovodov et al.[17] Experimental data for this case were taken from Settles and Dodson.[18]

Approach

Inflow Boundary Conditions

The proposed inflow boundary conditions are a particular extension of a rescaling-reintroducing procedure developed for LES simulations of compressible flows in Ref. 11. In many baseline experiments for testing the capability of high-speed turbulence models,[18] the inflow boundary layer is developed over a flat plate ahead of the various models. Thus, a procedure to provide turbulent inflow boundary conditions over a flat plate will have a wide range of possible applications.

The procedure of Ref. 11 consists of the following steps:

1) Extract mean values and fluctuating quantities from a downstream station, called the recycle plane.

2) Based on boundary-layer similarity, rescale the preceding values to account for boundary-layer growth.

3) Introduce the rescaled values at the inlet station as an updated boundary condition.

The hybrid approach differs from the LES approach of Ref. 11 by the existence of two additional equations for k and ζ and the existence of a blending function connecting LES and RANS closures. Thus, new and consistent similarity laws have to be derived to rescale all flow variables.

The development will proceed in two steps. The first addresses the velocity scaling for constant-wall and adiabatic-wall temperatures and is essentially identical to that of Ref. 11. The second is a new procedure, which addresses the scaling of the remaining variables: the density ρ, the temperature T, the turbulent kinetic energy per unit mass (variance of velocity fluctuations) k, and ζ the enstrophy (variance of vorticity fluctuations). Extension to other turbulence models is straightforward by utilizing relations among ζ and other turbulent quantities.

Let $u(x, y, z, t)$ denote the instantaneous velocity in the x-direction. It can be decomposed into two components:

$$u = U(x, y) + u''(x, y, z, t) \tag{1}$$

$$U = \frac{1}{t_f - t_i}\int_{t_i}^{t_f} \langle u\rangle \, \mathrm{d}t \tag{2}$$

where u'' is the instantaneous fluctuation. The operator $\langle\cdot\rangle$ stands for the average over the (assumed homogeneous) z direction. The multilayer scaling of a compressible boundary layer makes use of an effective velocity developed by van Driest.[19] The effective velocity is related to U by the relation

$$U_{\text{eff}} = \frac{U_\infty}{A_1}\left\{\sin^{-1}\left[\frac{2A_1^2(U/U_\infty) - A_2}{\sqrt{A_2^2 + 4A_1^2}}\right] + \sin^{-1}\left(\frac{A_2}{\sqrt{A_2^2 + 4A_1^2}}\right)\right\} \tag{3}$$

where

$$A_1 = \sqrt{\frac{(\gamma - 1)}{2} r M_\infty^2 \left(\frac{T_\infty}{T_w}\right)}, \qquad A_2 = \frac{T_{\text{aw}}}{T_w} - 1 \tag{4}$$

r is the recovery factor, γ is the ratio of specific heats, and the subscript aw refers to adiabatic wall, respectively.

By using the effective velocity, the similarity laws in the inner and outer regions can be written as

$$u_{\text{eff}}^{\text{inn}} = u_\tau f_1(y^+), \qquad y^+ = y u_\tau / \nu_w \tag{5}$$

$$u_{\text{eff}}^{\infty} - u_{\text{eff}}^{\text{out}} = u_\tau f_2(\eta), \qquad \eta = y/\delta \tag{6}$$

where y is the distance normal to the wall. The velocity fluctuations are related by

$$u_{\text{inf}}''^{\text{inn}} = \beta u_{\text{rec}}''^{\text{inn}}\left(y_{\text{inf}}^+, z, t\right) \tag{7}$$

$$u_{\text{inf}}''^{\text{out}} = \beta u_{\text{rec}}''^{\text{out}}(\eta_{\text{inf}}, z, t), \qquad \beta = \frac{u_{\tau,\text{inf}}}{u_{\tau,\text{rec}}} \tag{8}$$

Similar relations hold for the other velocity components.

The complete velocity fluctuation field is represented as the weighted average of inner and outer values and is given by[11,13]

$$u_{\text{inf}}'' = u_{\text{inf}}''^{\text{inn}}[1 - W(\eta_{\text{inf}})] + u_{\text{inf}}''^{\text{out}} W(\eta_{\text{inf}}) \tag{9}$$

where

$$W(\eta) = \frac{1}{2}\left\{1 + \tanh\left[\frac{4(\eta - B)}{(1 - 2B)\eta + B}\right]\right\} \qquad B = 0.2 \tag{10}$$

The variables β and $\delta_{\text{rec}}/\delta_{\text{inf}}$ are derived in Ref. 11 from a power law $u/u_\infty = (y/\delta)^{1/9}$ and are adopted here. Thus

$$\frac{\delta_{\text{rec}}}{\delta_{\text{inf}}} = \left(1 + 0.27\frac{L}{\delta_{\text{inf}}} Re_{\delta_{\text{inf}}}^{-\frac{1}{5}}\right)^{\frac{5}{6}} \tag{11}$$

$$\frac{u_{\tau,\text{rec}}}{u_{\tau,\text{inf}}} = \left(\frac{\delta_{\text{rec}}}{\delta_{\text{inf}}}\right)^{\frac{1}{10}} \tag{12}$$

where L is the distance between inflow and recycle planes.

We consider next the remaining inflow variables. Based on Morkovin's hypothesis,[20] the pressure fluctuations at moderately high-speed flows are negligible. Hence, the pressure at inflow is set equal to the freestream pressure p_∞. Thus, for this case the equation of state gives the density as a function of temperature. Therefore, we need to develop scaling laws for k, ζ, and T.

In the log–law region the convective, molecular diffusion, and viscous terms can be neglected. In this case the exact momentum and energy equations [see Eqs. (5.48) and (5.49) in Ref. 21] reduce to

$$\mu_t \frac{\mathrm{d}\tilde{u}}{\mathrm{d}y} = \tau_w = \bar{\rho}_w u_\tau^2 \tag{13}$$

$$\mu_t \frac{\mathrm{d}}{\mathrm{d}y}\left(\frac{C_p \tilde{T}}{Pr_t} + \frac{1}{2}\tilde{u}^2 + \frac{k}{\sigma_k}\right) = -q_w \tag{14}$$

where μ_t and Pr_t are the turbulent eddy viscosity and Prandtl number, C_p is the specific heat at constant pressure, σ_k is a model constant,[14] and q_w is the wall heat flux. For an insulated wall $q_w = 0$, and Eq. (14) reduces to

$$\frac{C_p}{Pr_t}(\tilde{T} - T_w) + \frac{\tilde{u}^2}{2} + \frac{k}{\sigma_k} = 0 \tag{15}$$

Thus, because $\tilde{u}$ scales with u_τ, k and $\tilde{T} - T_w$ will scale with u_τ^2. If q_w is not zero, then Eqs. (13) and (14) give

$$\frac{\mathrm{d}}{\mathrm{d}\tilde{u}}\left(\frac{C_p \tilde{T}}{Pr_t} + \frac{1}{2}\tilde{u}^2 + \frac{k}{\sigma_k}\right) = -\frac{q_w}{\rho_w u_\tau^2} \tag{16}$$

Because

$$q_w = -\frac{\mu C_p}{Pr}\left(\frac{\partial \tilde{T}}{\partial y}\right)_{y=0} = -\frac{C_p}{Pr}\tau_w \left(\frac{\partial \tilde{T}}{\partial \tilde{u}}\right)_{\tilde{u}=0} \tag{17}$$

then, q_w scales like u_τ^3.

Integration of Eq. (16) yields

$$\frac{\tilde{T}}{T_w} = \frac{\bar{\rho}_w}{\bar{\rho}} = 1 - (\gamma - 1) Pr_t M_\tau^2 \left[\frac{1}{2}\left(\frac{\tilde{u}}{u_\tau}\right) + \frac{q_w}{\bar{\rho}_w u_\tau^3}\left(\frac{\tilde{u}}{u_\tau}\right) + \frac{1}{\sigma_k}\left(\frac{k}{u_\tau^2}\right)\right] \tag{18}$$

where

$$M_\tau = \frac{u_\tau}{a_w} \tag{19}$$

and a_w is the speed of sound evaluated at the wall temperature. Thus, in the inner region the scaling laws are

$$\left(\frac{\tilde{T}}{T_w} - 1\right)_{\text{inf}}^{\text{inn}} = \beta^2 \left(\frac{\tilde{T}}{T_w} - 1\right)_{\text{rec}}^{\text{inn}} \tag{20}$$

$$\left(\frac{T''}{T_w}\right)_{\text{inf}}^{\text{inn}} = \beta^2 \left(\frac{T''}{T_w}\right)_{\text{rec}}^{\text{inn}} \tag{21}$$

$$k_{\text{inf}}^{\text{inn}} = \beta^2 k_{\text{rec}}^{\text{inn}} \tag{22}$$

The turbulent eddy viscosity in the log–law region is given by

$$\nu_t = \kappa u_\tau y, \qquad \kappa = 0.4 \tag{23}$$

Because

$$\nu_t = C_\mu \frac{k^2}{\nu\zeta}, \qquad C_\mu = 0.09 \tag{24}$$

ζ scales in the inner region as

$$\left(\frac{\nu\nu_w\zeta}{u_\tau^4}\right)_{\text{inf}}^{\text{inn}} = \left(\frac{\nu\nu_w\zeta}{u_\tau^4}\right)_{\text{rec}}^{\text{inn}} \tag{25}$$

In the outer region it is assumed that

$$\left(\frac{T''}{T_w}\right)_{\text{inf}}^{\text{out}} = \beta^2 \left(\frac{T''}{T_w}\right)_{\text{rec}}^{\text{out}} \tag{26}$$

Based on Wilcox's analysis of the outer region [see Eq. (4.162) of Ref. 21], k and ζ scale like

$$k_{\text{inf}}^{\text{out}} = \beta^2 k_{\text{rec}}^{\text{out}} \tag{27}$$

and as

$$\left(\frac{\delta\nu\zeta}{u_\tau^3}\right)_{\text{inf}}^{\text{out}} = \left(\frac{\delta\nu\zeta}{u_\tau^3}\right)_{\text{rec}}^{\text{out}} \tag{28}$$

Though this procedure accounts for the rescaling of both mean and fluctuating components, we have found that rescaling mean values can be problematic for high-Reynolds-number flows, as "drift" in boundary-layer properties can occur over time, leading to a failure to reach a statistically stationary state. A similar observation was made independently in Ref. 22, who tested several rescaling-reintroducing techniques for compressible flows and found that all exhibited boundary-layer drift to varying degrees. Our solution, as well as that of Ref. 22, is to obtain mean velocity and temperature profiles at the inflow plane from a separate source, such as a RANS solver or a boundary-layer code, and recycle only the fluctuation field. The current rescaling-reintroducing method can be thus summarized as follows:

1) Fix the mean profiles of velocity and temperature at inflow. The mean static pressure is set at p_∞, and the mean density is determined from the equation of state.

2) Extract fluctuations of velocity, temperature, and density at the recycle station.

3) Rescale the fluctuations according to the preceding scaling laws, and superimpose them at every time step onto the mean inflow profiles.

4) Rescale and recycle both mean and fluctuating values of k and ζ according to the preceding rules.

Turbulent Closure

The LES/RANS hybrid scheme is similar to the that developed in Refs. 6 and 8. The k equation in the k–ζ model can be written as[14]

$$\frac{\partial\bar{\rho}k}{\partial t} + \frac{\partial\bar{\rho}\tilde{u}_j k}{x_j} = \frac{\partial}{\partial x_j}\left[\left(\frac{\mu}{3} + \frac{\mu_t}{\sigma_k}\right)\frac{\partial k}{\partial x_j}\right] + \tau_{ij}\frac{\partial\tilde{u}_i}{\partial x_j} - \frac{1}{C_k}\frac{\mu_t}{\bar{\rho}^2}\frac{\partial\bar{\rho}}{\partial x_i}\frac{\partial\bar{P}}{\partial x_i} - C_1\frac{\bar{\rho}k}{\tau_\rho} - \mu\zeta \tag{29}$$

In this model the RANS kinematic eddy viscosity $\nu_{t,\text{RANS}}$ is given by Eq. (24), whereas the LES kinematic eddy viscosity is defined as

$$\nu_{t,\text{LES}} = C_s\sqrt{k}\Delta \tag{30}$$

where

$$\Delta = \Delta_m = \max(\Delta_x, \Delta_y, \Delta_z) \tag{31}$$

or

$$\Delta = \Delta_v = (V_{\text{cell}})^{\frac{1}{3}} \tag{32}$$

In this, Δ_x is the mesh spacing in the x direction, etc.; C_s is a model constant; and V_{cell} is the local cell volume. If the dissipation term in the LES region is chosen as

$$C_d\bar{\rho}\frac{k^{\frac{3}{2}}}{\Delta} \tag{33}$$

where C_d is a model constant, then the k equation for the hybrid LES/RANS scheme is

$$\frac{\partial\bar{\rho}k}{\partial t} + \frac{\partial\bar{\rho}\tilde{u}_j k}{\partial x_j} = \frac{\partial}{\partial x_j}\left[\left(\frac{\mu}{3} + \frac{\mu_t}{\sigma_k}\right)\frac{\partial k}{\partial x_j}\right] + \tau_{ij}\frac{\partial\tilde{u}_i}{\partial x_j} - (1-\Gamma)\left(\frac{1}{C_k}\frac{\mu_t}{\bar{\rho}^2}\frac{\partial\bar{\rho}}{\partial x_i}\frac{\partial\bar{P}}{\partial x_i} + C_1\frac{\bar{\rho}k}{\tau_\rho} + \mu\zeta\right) - \Gamma C_d\bar{\rho}\frac{k^{\frac{3}{2}}}{\Delta} \tag{34}$$

where

$$\nu_t = (1-\Gamma)\nu_{t,\text{RANS}} + \Gamma\nu_{t,\text{LES}}, \qquad \Gamma = \tanh\left(\frac{l_\epsilon}{\alpha_1\Delta}\right)^2$$

$$l_\epsilon = \frac{k^{\frac{3}{2}}}{\nu\zeta} \tag{35}$$

When $l_\epsilon \ll \alpha_1\Delta$, $\Gamma \to 0$, and Eq. (34) reverts to Eq. (29). On the other hand, when $\Gamma \to 1$, Eq. (34) provides a subgrid-scale model for LES. When production balances dissipation in the LES region, Eq. (34) yields a Smagorinsky-type subgrid eddy viscosity

$$\nu_t \sim C_s\sqrt{\frac{C_s}{C_d}}(S_{ij}S_{ij})^{\frac{1}{2}}, \qquad S_{ij} = \frac{1}{2}\left(\frac{\partial u_i}{\partial x_j} + \frac{\partial u_j}{\partial x_i}\right) \tag{36}$$

Both C_s and C_d are chosen as 0.01 in this work.[6,8]

Note that for the assumed eddy viscosities

$$\frac{l_\epsilon}{\alpha_1\Delta} \sim \frac{\nu_{t,\text{RANS}}}{\nu_{t,\text{LES}}} \tag{37}$$

Numerical Procedure

The numerical scheme for solving the hybrid LES/RANS system is similar to that used in Refs. 6 and 8. A second-order essentially

nonoscillatory upwind method based on the low-diffusion flux-splitting scheme of Edwards[23] is used to discretize the inviscid fluxes, whereas central differences are employed for the viscous and diffusion terms. A planar relaxation subiteration procedure that results in second-order temporal accuracy is used to integrate the system. The code is parallelized using domain-decomposition and message-passing-interface strategies and is optimized for the IBM SP3 architecture in place at the North Carolina Supercomputing Center.

Results and Discussion

Flat Plate

The inflow fluctuation–generation method was tested first for a flow over a flat plate. The dimensions of the plate are $0.1 \times 0.092 \times 0.087$ m. The grid size is $129 \times 129 \times 65$ in the flow, normal, and crossflow directions. The entire domain is decomposed into $8 \times 4 \times 2$ blocks. The recycle plane is located six cells upstream of the outflow boundary. The test conditions are those used for the 20-deg-ramp calculation of Ref. 8 and are given in Table. 1.

It turns out that there are a number of ways that the inflow boundary conditions and blending functions can be implemented. The criterion used in selecting a proper procedure is to monitor the solution at the recycle plane and to require that a statistically steady turbulent flow develop there over time. A number of approaches were explored. The most satisfactory results were obtained by fixing the mean flow conditions at the inflow plane and rescaling reintroducing only the fluctuation fields, as discussed earlier. Furthermore, it was found necessary to force the the blending function to be a nondecreasing function as the distance from the wall increases. For the simple grids used in this study, this was implemented by requiring that

$$\Gamma_j = \max(\Gamma_j, \Gamma_{j-1}) \tag{38}$$

where j is the index of the grid cell in the normal direction. For complex shapes the preceding requirement can be met by keeping track of the normal distance to the nearest wall.

Figures 1 and 2 show profiles of Γ and μ_t at the recycle plane when Eq. (38) is not enforced, whereas Figs. 3 and 4 show the same

Table 1 Inflow conditions for flat-plate flow

Parameter	Value
M_∞	2.79
P_∞, Pa	26,001
T_∞, K	100.8
ρ_∞, kg/m^3	0.77
Re/m	7.2×10^7
δ, cm	3.0

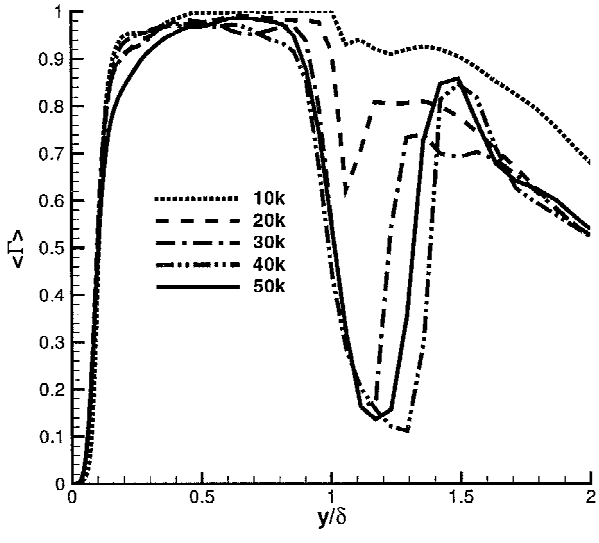

Fig. 1 Profiles of blending function Γ.

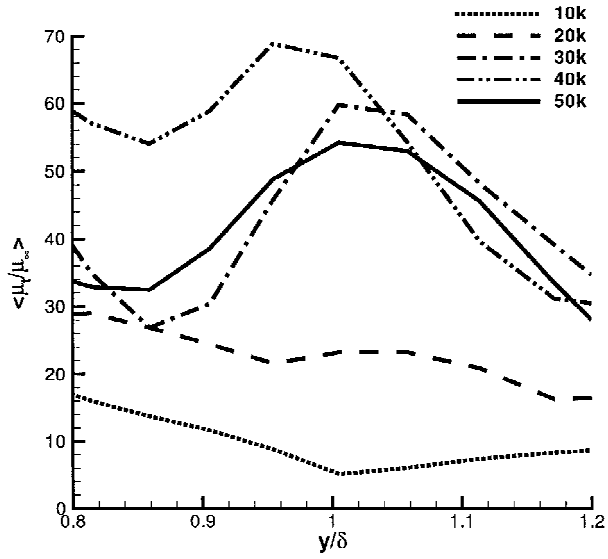

Fig. 2 Profiles of eddy viscosity at the edge of boundary layer.

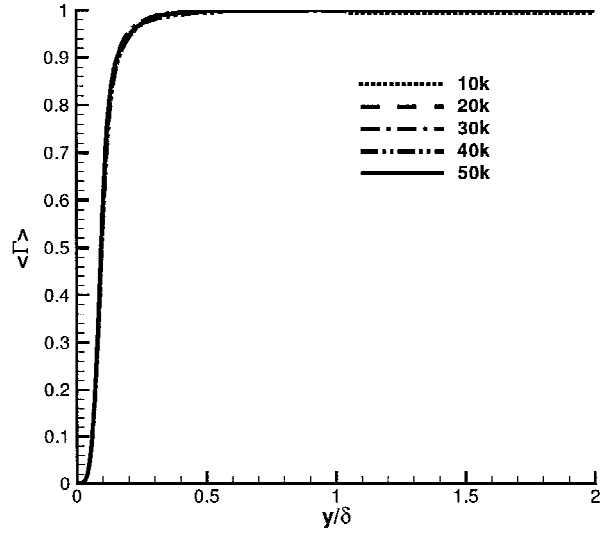

Fig. 3 Profiles of blending function Γ.

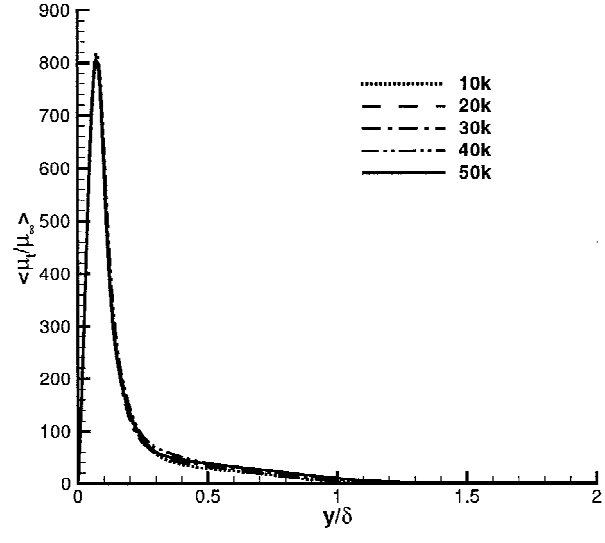

Fig. 4 Profiles of eddy viscosity.

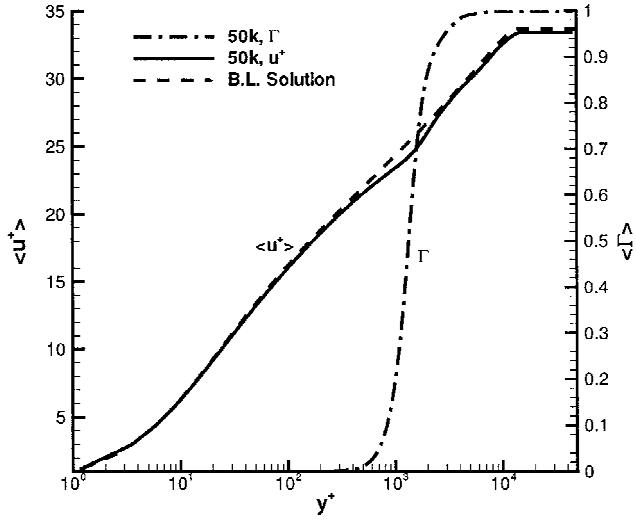

Fig. 5 Profiles of u^+ and Γ.

quantities when Eq. (38) is enforced. It is clear that statistically steady solutions were not obtained in Figs. 1 and 2 even after 50,000 iterations, whereas statistically steady solutions were obtained after 10,000 iterations in Figs. 3 and 4. All of the calculations were carried out for $\Delta = \Delta_m$ and a value of $\alpha_1 = 5$. The value of α_1 determines the location where transition from a RANS region to an LES region takes place. The choice of $\alpha_1 = 5$ ensures that the transition takes place within the log layer. Figure 5 shows a plot of u^+ and Γ vs y^+. It is seen that the resulting solution agrees well with the profile calculated from a RANS code. Figures 6 and 7 show contour plots of instantaneous temperature on the x–y and y–z planes, respectively. Periodic boundary conditions are employed in the z direction in all calculations presented here.

25-deg Compression–Expansion Ramp[17,18]

The schematic of the experiment together with relevant dimensions is shown in Fig. 8. Two grids were employed in this investigation: a coarse grid that consists of $361 \times 109 \times 65$ nodes in the flow, normal, and spanwise directions; and a fine mesh that consists of $481 \times 145 \times 65$ nodes. Both grids are uniformly spaced in the x and z directions and are heavily clustered in the y direction, with $y^+ < 1$

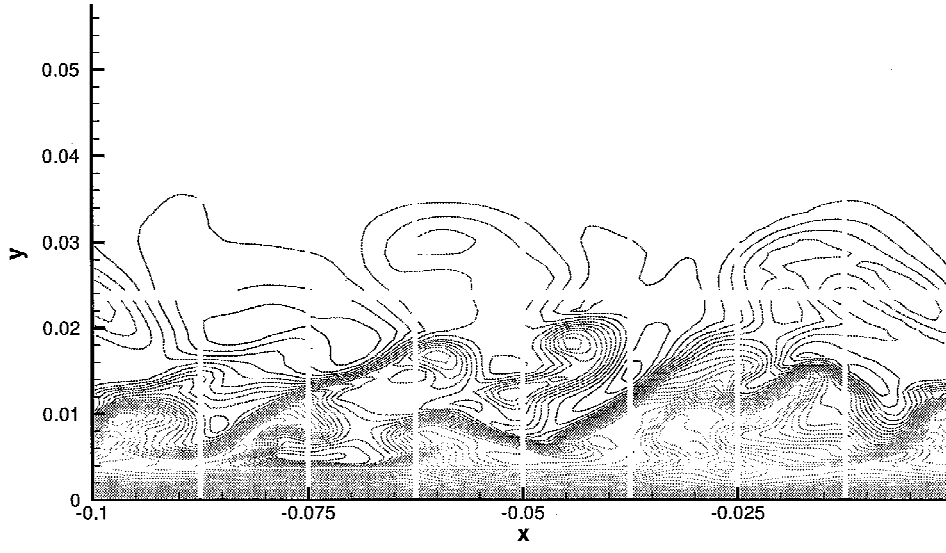

Fig. 6 Instantaneous temperature in x–y plane.

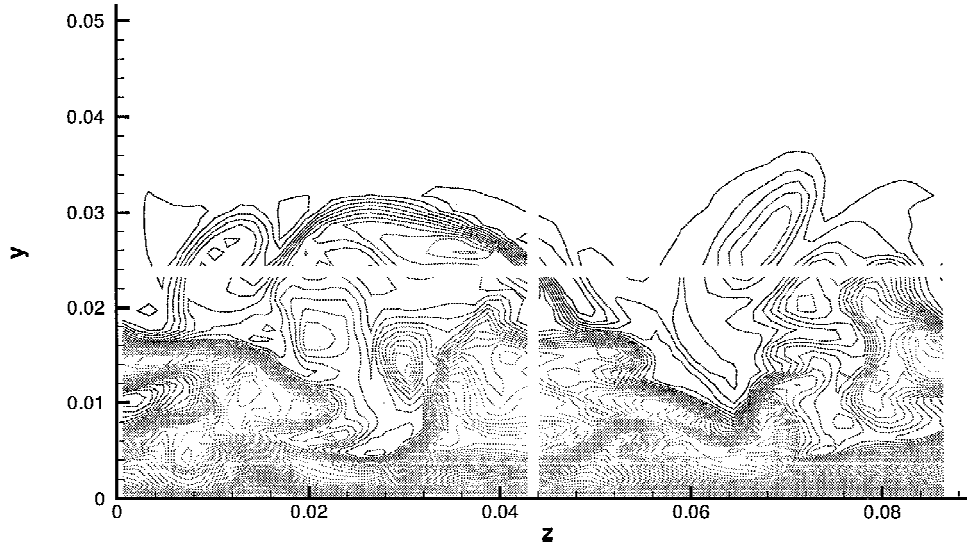

Fig. 7 Instantaneous temperature in y–z plane.

Table 2 Inflow condition at $x = -3.3$ cm (25-deg compression–expansion ramp)

Parameter	Value
M_∞	2.88
P_∞, Pa	11,956
T_∞, K	114.8
ρ_∞, kg/m^3	0.36
Re/m	3.24×10^7
θ, mm	0.3
δ, mm	4.1

for the center of the first cell off the wall. In both cases the physical size of the grid in the z direction is 2.9δ. The whole domain is decomposed into $12 \times 4 \times 2$ equal-size blocks and solved on 96 processors using the IBM SP3. The inflow conditions at $x = -3.3$ cm are presented in Table 2. A two-dimensional RANS code was used to obtain a steady-state solution, and the inflow-plane profile was selected by matching the computed momentum thickness with the experimental value. The same geometry was the subject of a large-eddy simulation conducted by Urbin et al.[24] at $Re_\delta = 2 \times 10^4$. Based on the conditions indicated in Table 2, this Reynolds number is about one order of magnitude lower than that of the experiment.

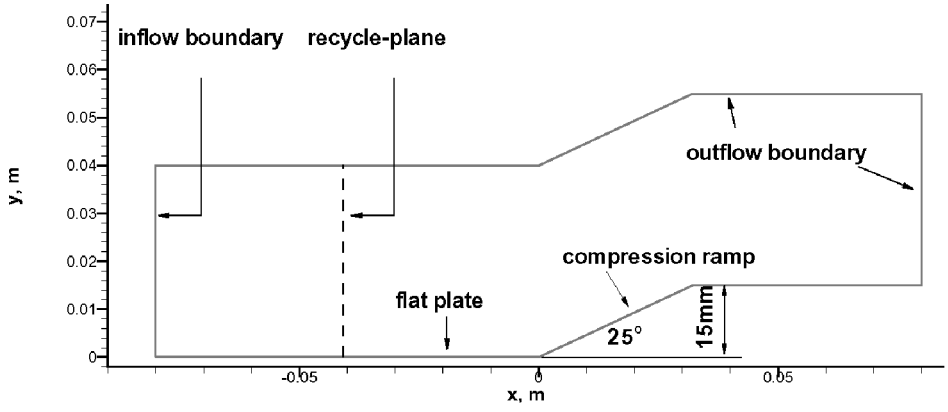

Fig. 8 Zheltovodov 25-deg compression–expansion ramp.

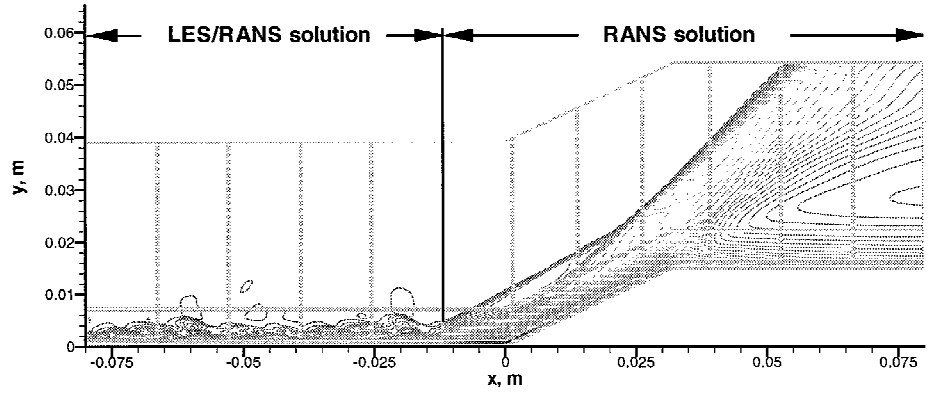

Fig. 9 Combined initial solution: contour plot of u.

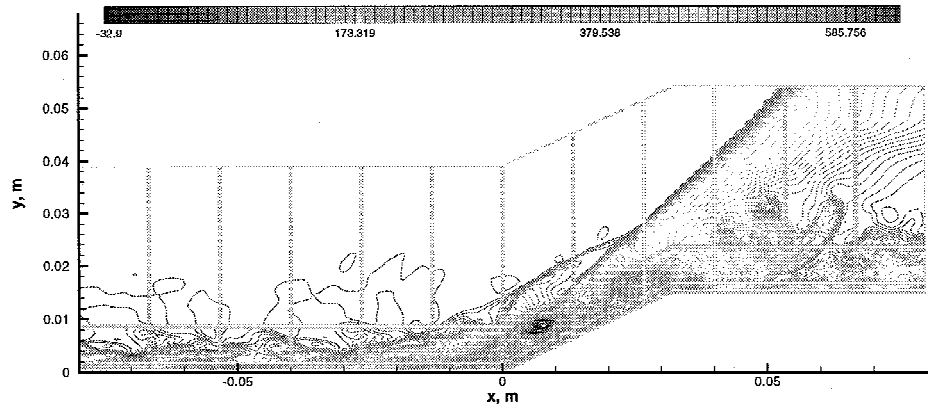

Fig. 10 Instantaneous streamwise velocity u distribution.

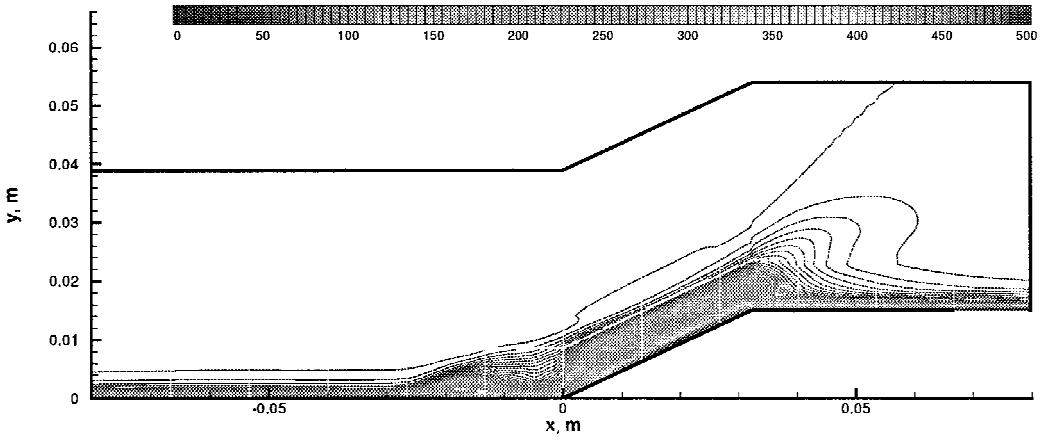

a) $\mu_t/\mu_\infty, \Gamma_1$

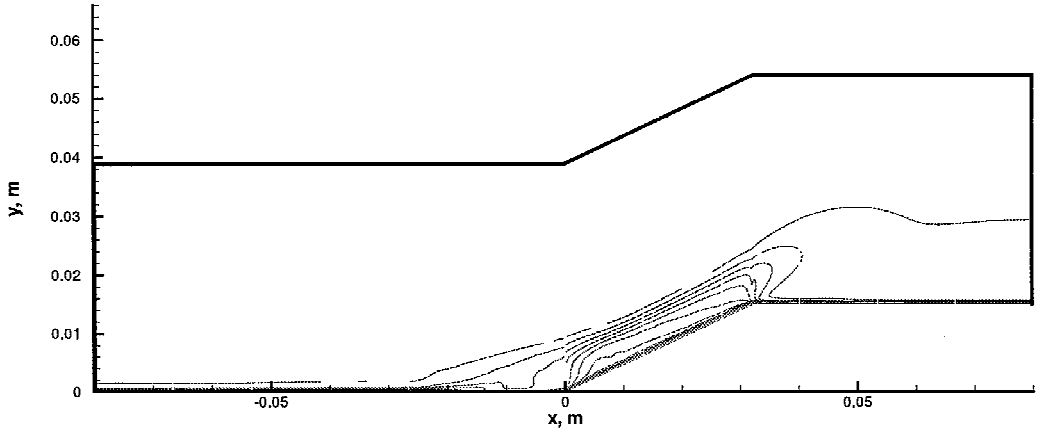

b) $\mu_t/\mu_\infty, \Gamma_2$

Fig. 11 Mean eddy viscosity distribution.

As shown by Fan et al.,[15] it might be difficult to induce a proper LES/RANS response for shock/boundary-layer interactions if one starts from a steady RANS solution without significant structural content. One reason is that, in the absence of RANS levels of eddy viscosity, the separation zone can feed forward, eventually contaminating the recycling plane. To avoid this problem, a new starting procedure is developed. In this procedure an initial solution for the flat plate part is generated separately, using the procedure just outlined, whereas the region downstream of the corner is initialized by the RANS solution. A representative starting profile is shown in Fig. 9, which shows the instantaneous velocity u distribution.

The initial flat-plate solution does not need to have reached a statistically steady state, as the flat-plate flow will evolve further as part of the combined flat-plate/ramp solution. One can monitor the rms mass flux fluctuations, that is,

$$\sqrt{\overline{\langle \rho u'' \rangle^2}} \approx \sqrt{\overline{\langle \rho u \rangle^2} - \overline{\langle \rho u \rangle}^2} \tag{39}$$

at the recycle plane and use the resulting solution as the initial solution when the preceding quantity is about $0.08\rho_\infty u_\infty$.

Two sets of calculations were carried out. In the first, $\Delta = \Delta_m$, and the corresponding Γ is labeled as Γ_1. In the second, $\Delta = \Delta_v$, and the corresponding Γ is labeled as Γ_2. Results from these two sets of calculations, which represent average values over 40,000 iterations, are presented and compared with the RANS $k-\zeta$ solution and with experimental data. It should be noted that 10,000 iterations correspond to 2.3 characteristic times, which is the time it takes for a particle to traverse the domain with a velocity equal to the freestream velocity.

Figure 10 shows a typical instantaneous streamwise velocity distribution after 40,000 iterations. The large size of eddies in the incoming boundary layer is evident. Other features in this flow include the leading shock wave generated by the flow separation around the compression corner and an embedded shock wave caused by the flow reattachment onto the ramp surface.

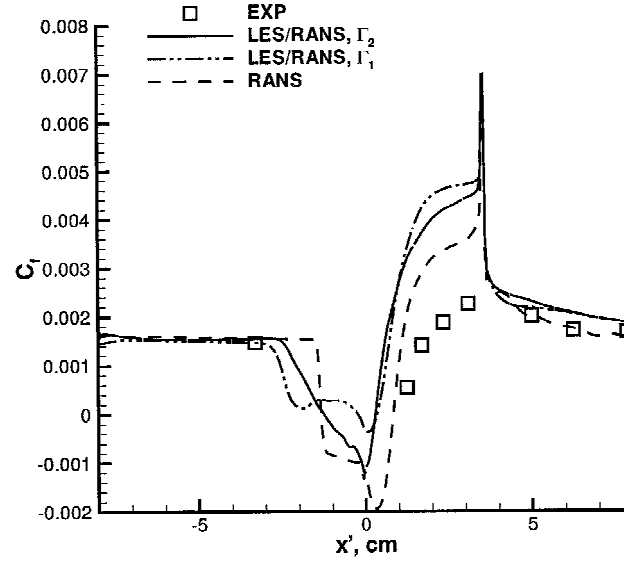

Fig. 12 Skin-friction distribution.

Time-averaged eddy viscosity contours in Fig. 11 indicate that the Γ_2 scheme is characterized by a lower eddy viscosity. This means that the LES/RANS juncture is shifted closer to the wall, and more of the flow is modeled using the LES strategy. Figures 12–14 compare

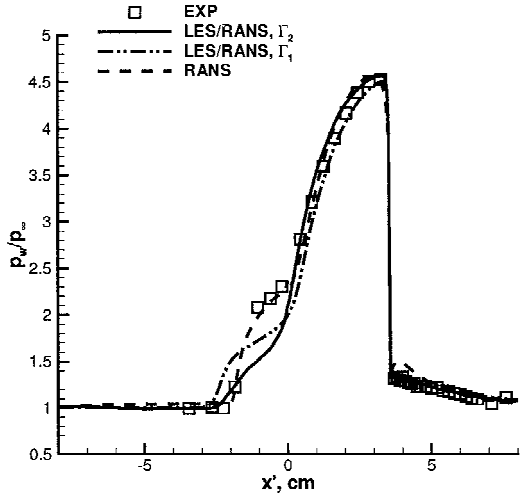

Fig. 13 Wall-pressure distribution.

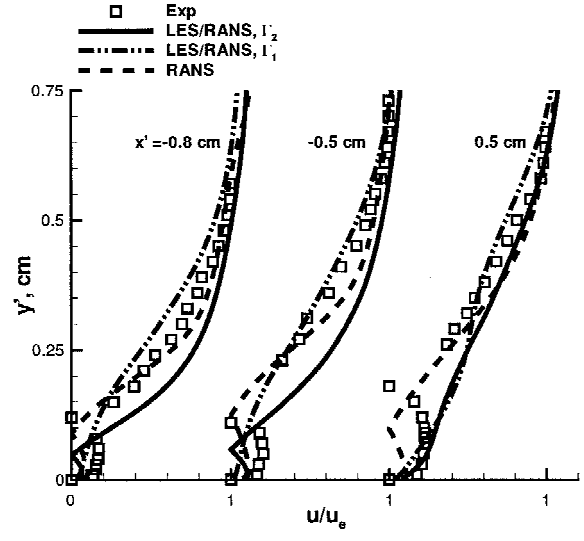

a) Separation region

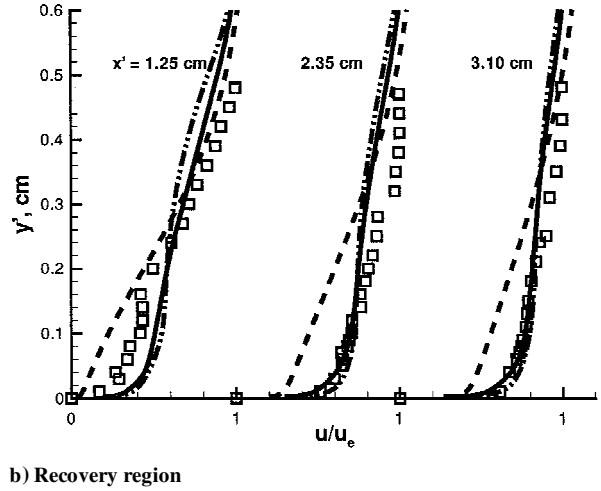

b) Recovery region

Fig. 14 Comparison of velocity profiles for the coarse grid.

predictions of skin-friction coefficient, surface pressure, and velocity profiles with experimental data. As shown in Fig. 12, the Γ_2 scheme predicts a smaller region of axial separation and gives a lower skin friction in the recovery region, compared with the Γ_1 scheme. Figure 13 shows that the Γ_2 scheme results in a lower pressure in the separation region, indicating that the initial displacement effect of the separation bubble is not as pronounced as in the RANS calculation or in the Γ_1 scheme. The upstream extent of axial

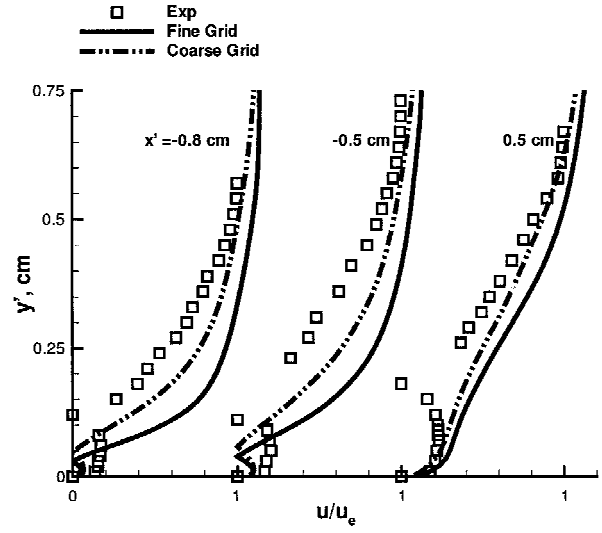

a) Separation region

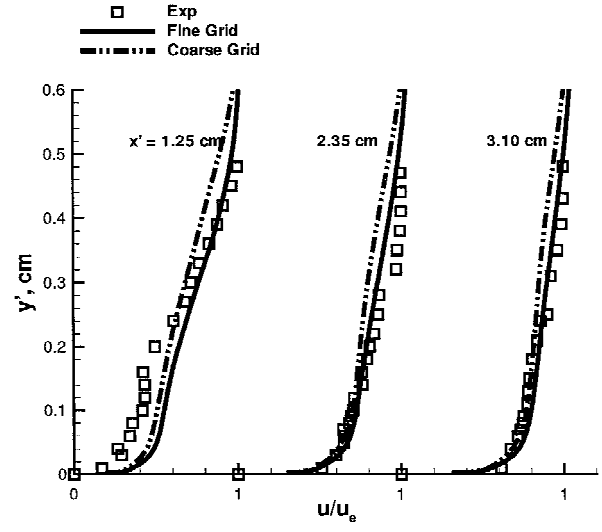

b) Recovery region

Fig. 15 Effect of grid refinement on velocity profiles: Γ_2 scheme.

separation is overpredicted by the Γ_1 scheme, whereas the Γ_2 scheme and the RANS calculation yield reasonable agreement with the experimental data. Overall, neither hybrid strategy shows as good of an agreement with experimental data as does the RANS k–ζ model.

Figure 14 compares predicted axial velocity magnitude profiles within the separation and recovery regions with experimental data. The experimental data do not indicate negative axial velocities, but it can be assumed that the "cusps" evident in the profiles upstream of the ramp apex delineate the outer edge of the backflow region. In the figure $y' = y - y_{\text{wall}}$, and x' is measured along the surface from the corner of the compression ramp. The Γ_2 scheme, where the LES region is larger, resolves the inner backflow structure in the two stations upstream of the compression corner, but the Γ_1 scheme does not. At the station downstream of the corner($x' = 0.5$ cm), none of the hybrid schemes is able to predict the backflow structure. The RANS solution predicts the structure, but the size of the backflow region is not as large as that found in the experiment. On the other hand, the hybrid schemes predict the rapid recovery of the inner part of the boundary layer downstream of reattachment, especially close to the wall. The RANS model severely underpredicts the recovery rate.

A grid-refinement study was carried out for the Γ_2 scheme, with the resolution increasing from $361 \times 109 \times 65$ nodes to $481 \times 145 \times 65$ nodes. Insignificant differences were found for the skin-friction and pressure distributions. However, Fig. 15 shows

some differences in the velocity profiles within the separation region. The inflow boundary layer is more energetic when the grid is refined, and this results in a slight shrinking of the separation region. In the recovery region, grid refinement results in better agreement with experiment, especially in the outer region of the boundary layer.

Conclusions

In this study a rescaling-reintroducing method for generating turbulent inflow conditions has been modified and extended for use with large-eddy simulation/Reynolds-averaged Navier–Stokes (LES/RANS) hybrid schemes. By using monotone blending functions and by only recycling the fluctuation field, the modified procedure is capable of generating the necessary turbulence structure and maintaining the desired mean inflow profiles.

Using this method, the scheme has been used to simulate Zheltovodov's 25-deg compression–expansion ramp experiment. To prevent the initial rapid growth of the separation bubble when starting from a RANS solution (but with subgrid levels of eddy viscosity), a special starting procedure has been implemented. In this procedure a hybrid LES/RANS solution for the flat-plate portion of the configuration is coupled with a RANS solution for the ramp portion to initialize the whole flowfield. The advantage of this procedure is that it can effectively keep the initial separation bubble from reaching the recycle plane so that the inflow fluctuation–generation procedure can work properly without downstream influence.

Although the hybrid schemes did not show much improvement over the RANS scheme in the separated region, much improvement is indicated in the recovery region. Because flows in separated region might be highly unsteady in the mean, part of the discrepancy might be a result of differences in determining mean values in the experiment and computation. Analysis of the probability density functions of the shock-wave motion frequency reveals that the mean location of the shock wave determined from mean surface pressure is quite different from the most probable value. This might explain the source of the discrepancy in the separated region.

The present work demonstrates that hybrid LES/RANS methods can work well for supersonic separated flows in which there is no clear demarcation between LES and RANS regions. Moreover, it provides a way for LES methods to address complex flows at high Reynolds numbers.

Acknowledgments

This research is sponsored in part by Taitech, Inc., under Contract F33615-00-C-2017. Xudong Xiao acknowledges the support of North Carolina State University. IBM SP3 computer time is provided by a grant from the North Carolina Supercomputing Center.

References

[1]Speziale, C. G., "Turbulence Modeling for Time-Dependent RANS and VLES: A Review," *AIAA Journal*, Vol. 36, No. 2, 1998, pp. 173–184.

[2]Spalart, P. R., Jou, W.-H., Strelets, M., and Allmaras, S., "Comments on the Feasibility of LES for Wings and on a Hybrid RANS/LES Approach," *Advances in DNS/LES*, edited by C. Liu and Z. Liu, Greyden Press, Columbus, OH, 1997, pp. 137–147.

[3]Batten, P., Goldberg, U. C., and Chakravarthy, S. R., "Sub-Grid Turbulence Modeling for Unsteady Flow with Acoustic Resonance," AIAA Paper 2000-0473, Jan. 2000.

[4]Arunajatesan, S., and Sinha, N., "Unified Unsteady RANS–LES Simulation of Cavity Flowfields," AIAA Paper 2001-0516, Jan. 2001.

[5]Strelets, M., "Detached Eddy Simulation of Massively Separated Flows," AIAA Paper 2001-0879, Jan. 2001.

[6]Fan, T. C., Tian, M., Edwards, J. R., Hassan, H. A., and Baurle, R. A., "Validation of a Hybrid Reynolds-Averaged/Large-Eddy Simulation Method for Simulating Cavity Flameholder Configuration," AIAA Paper 2001-2929, June 2001.

[7]Bush, R., and Mani, M., "A Two-Equation Large-Eddy Stress Model for High Sub-Grid Shear," AIAA Paper 2001-2561, June 2001.

[8]Fan, T. C., Xiao, X., Edwards, J. R., Hassan, H. A., and Baurle, R. A., "Hybrid LES/RANS Simulation of a Shock Wave/Boundary Layer Interaction," AIAA Paper 2002-0431, Jan. 2002.

[9]Batten, P., Goldberg, U., and Chakravarthy, S., "LNS—An Approach Towards Embedded LES," AIAA Paper 2002-0427, Jan. 2002.

[10]Arunajatesan, S., Kannepalli, C., and Dash, S. M., "Progress Towards Hybrid RANS-LES Modeling for High Speed Flow," AIAA Paper 2002-0482, Jan. 2002.

[11]Urbin, G., and Knight, D., "Large-Eddy Simulation of a Supersonic Boundary Layer Using an Unstructured Grid," *AIAA Journal*, Vol. 39, No. 7, 2001, pp. 1288–1295.

[12]Spalart, P. R., and Leonard, A., "Direct Numerical Simulation of Equilibrium Turbulent Boundary Layers," *Proceedings of the 5th Symposium on Turbulent Shear Flows*, edited by F. Durst, B. E. Launder, J. L. Lumley, F. W. Schmitd, and J. H. Whitelaw, Springer-Verlag, Berlin, 1987, pp. 234–252.

[13]Lund, T. S., Wu, X., and Squires, K. D., "Generation of Turbulent Inflow Data for Spatially-Developing Boundary Layer Simulation," *Journal of Computational Physics*, Vol. 140, 1998, pp. 233–258.

[14]Robinson, D. F., and Hassan, H. A., "Further Development of the k–ζ (Enstrophy) Turbulence Closure Model," *AIAA Journal*, Vol. 36, No. 10, 1998, pp. 1825–1833.

[15]Fan, T., Xiao, X., Edwards, J., Hassan, H., and Baurle, R., "Hybrid LES/RANS Simulation of a Mach 3 Shock Wave/Boundary Layer Interaction," AIAA Paper 2003-0080, Jan. 2003.

[16]Menter, F. R., "Two-Equation Eddy-Viscosity Turbulence Models for Engineering Applications," *AIAA Journal*, Vol. 32, No. 8, 1994, pp. 1598–1605.

[17]Zheltovodov, A. A., Zaulichnii, E. G., Trofimov, V. M., and Yakolev, V. N., "Heat Transfer and Turbulence Study in Compressible Separated Flows," Preprint 22-87, Inst. Theoretical and Applied Mechanics, Russian Academy of Sciences, Novosobirsk, Russia, 1987.

[18]Settles, G. S., and Dodson, L. J., "Hypersonic Shock/Boundary-Layer Interaction Database," NASA CR 177577, April 1991.

[19]van Driest, E. R., "Turbulent Boundary Layer in Compressible Fluids," *Journal of Aeronautical Sciences*, Vol. 18, No. 2, 1951, pp. 145–160.

[20]Morkovin, M. V., "Effects of Compressibility in Turbulence Flow," *The Mechanics of Turbulence*, edited by A. Favre, Gordon and Breach, New York, 1962.

[21]Wilcox, D. C., *Turbulence Modeling for CFD*, 2nd ed., DCW Industries, La Canada, CA, 1998, Chap. 5.

[22]Sagaut, P., Garnier, E., Tromeur, E., Larcheveque, E., and Labourasse, L., "Turbulent Inflow Conditions for LES of Supersonic and Subsonic Wall-Bounded Flows," AIAA Paper 2003-0068, Jan. 2003.

[23]Edwards, J. R., "A Low Diffusion Flux Splitting Scheme for Navier–Stokes Calculations," *Computers and Fluids*, Vol. 26, No. 6, 1997, pp. 635–659.

[24]Urbin, G., Knight, D., and Zheltovodov, A. A., "Large Eddy Simulation of a Supersonic Compression Corner Part I," AIAA Paper 2002-0398, Jan. 2002.

R. M. C. So
Associate Editor